



# MIT Open Access Articles

## *Long-term rainfall risk from tropical cyclones in coastal areas*

The MIT Faculty has made this article openly available. **Please share** how this access benefits you. Your story matters.

<b>Citation</b>	Langousis, Andreas, and Daniele Veneziano. "Long-term Rainfall Risk from Tropical Cyclones in Coastal Areas." <i>Water Resources Research</i> 45.11 (2009). © 2009 John Wiley & Sons, Inc.
<b>As Published</b>	<a href="http://dx.doi.org/10.1029/2008wr007624">http://dx.doi.org/10.1029/2008wr007624</a>
<b>Publisher</b>	American Geophysical Union (Wiley platform)
<b>Version</b>	Final published version
<b>Citable link</b>	<a href="http://hdl.handle.net/1721.1/77990">http://hdl.handle.net/1721.1/77990</a>
<b>Terms of Use</b>	Article is made available in accordance with the publisher's policy and may be subject to US copyright law. Please refer to the publisher's site for terms of use.

## Long-term rainfall risk from tropical cyclones in coastal areas

Andreas Langousis<sup>1</sup> and Daniele Veneziano<sup>1</sup>

Received 28 November 2008; revised 18 May 2009; accepted 27 July 2009; published 26 November 2009.

[1] We develop a methodology for the frequency of extreme rainfall intensities caused by tropical cyclones (TCs) in coastal areas. The model does not account for landfall effects. This makes the developed framework best suited for open water sites and coastal areas with flat topography. The mean rainfall field associated with a TC with maximum tangential wind speed  $V_{\max}$ , radius of maximum winds  $R_{\max}$ , and translation speed  $V_t$  is obtained using a physically based model, whereas rainfall variability at both large scales (from storm to storm) and small scales (due to rainbands and local convection) is modeled statistically. The statistical component is estimated using precipitation radar data from the Tropical Rainfall Measuring Mission. Taylor's hypothesis is used to convert spatial rainfall intensity fluctuations to temporal fluctuations at a given location A. The combined physical-statistical model gives the distribution of the maximum rainfall intensity at A during an averaging period  $D$  for a TC with characteristics  $(V_{\max}, R_{\max}, V_t)$  that passes at a given distance from A. To illustrate the use of the model for long-term rainfall risk analysis, we formulate a recurrence model for tropical cyclones in the Gulf of Mexico that make landfall between longitudes  $85^\circ$  and  $95^\circ$ W. We then use the rainfall and recurrence models to assess the rainfall risk for New Orleans. For return periods of 100 years or more and long averaging durations ( $D$  around 12–24 h), tropical cyclones dominate over other rainfall event types, whereas the reverse is true for shorter return periods or shorter averaging durations.

**Citation:** Langousis, A., and D. Veneziano (2009), Long-term rainfall risk from tropical cyclones in coastal areas, *Water Resour. Res.*, 45, W11430, doi:10.1029/2008WR007624.

### 1. Introduction

[2] The quantification of long-term rainfall risk is a basic problem of stochastic hydrology [e.g., Chow *et al.*, 1988; Singh, 1992]. Our specific interest is in the risk of extreme rainfall posed at coastal sites by tropical cyclones (TCs). These events are relatively rare, but in combination with wind, surge and waves, high rainfall intensities may have devastating consequences [Herbert *et al.*, 1997; Rappaport, 2000].

[3] For ordinary rainfall, standard risk analysis techniques use historical annual-maximum data [e.g., Koutsoyiannis *et al.*, 1998] or peak-over-threshold (POT) information [e.g., Madsen *et al.*, 1997]. The episodic and spatially localized nature of tropical cyclones prevents one from using these standard techniques. For example, the annual maximum and POT rainfall statistics due to tropical cyclones are very sensitive to whether the site is “hit” by one or more TCs during a year and therefore are highly erratic. For this reason, the risk is best assessed parametrically, by combining a probabilistic model of the maximum rainfall due to a TC with given characteristics  $\theta = [\theta_1, \dots, \theta_r]$  with the rate at which those events occur. For coastal sites, the vector  $\theta$  might include the intensity and size of the storm, the location and

translational velocity at landfall, and possibly other parameters related to atmospheric conditions, the radial profile of the tangential winds, etc. Parametric approaches of this type have been used to assess the risk posed by tropical cyclones for wind, surge and waves [Myers, 1975; Ho and Myers, 1975; Ho *et al.*, 1987; Powell *et al.*, 2005; Interagency Performance Evaluation Taskforce (IPET), 2006, 2008], but not rain. Here we develop a parametric approach to calculate peak rainfall intensities from tropical cyclones, and use this approach to study the importance of TCs relative to other storm types and determine the TC characteristics that dominate different levels of risk.

[4] The main problem for rainfall is to evaluate the extreme precipitation intensities caused by a TC with given characteristics  $\theta$ . The historical data are too sparse and the potentially important TC parameters are too many to infer such extreme rainfalls from empirical observations alone. For example, current empirical approaches [Lonfat *et al.*, 2004, 2007; Tuleya *et al.*, 2007] classify storms into three coarse intensity categories and use microwave imager (TMI) data from the Tropical Rainfall Measuring Mission (TRMM) [Simpson *et al.*, 1988] to calculate the ensemble-average rainrate for each category as a function of distance from the TC center.

[5] The alternative we pursue here is to use a physical model to assess the dependence of the mean rainfall field on  $\theta$  and statistical analysis to quantify the fluctuations of rainfall intensity around this mean field. The physical model is that developed by Langousis *et al.* [2008] and Langousis and Veneziano [2009]. Langousis *et al.* [2008] proposed a

<sup>1</sup>Department of Civil and Environmental Engineering, Massachusetts Institute of Technology, Cambridge, Massachusetts, USA.

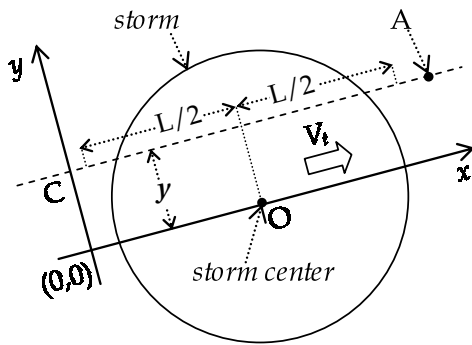


**Figure 1.** Schematic representation of a moving storm. Point O translates with the storm at speed  $V_t$ . Point A is the geographical location of interest.

theoretical method to estimate the large-scale horizontal and vertical winds inside TCs (the vertical winds are largely responsible for rain). The model is an extension of *Smith's* [1968] formulation and is referred to here as the Modified Smith (MS) model. Characteristics of the TC that are explicitly considered by the model are the maximum tangential wind speed  $V_{\max}$ , the radius of maximum winds  $R_{\max}$ , the parameter  $B$  that controls the shape of the radial profile of the tangential wind speed [Holland, 1980], the storm translation velocity  $V_t$ , the surface drag coefficient  $C_d$ , and the vertical diffusion coefficient  $K$ . When  $V_t = 0$ , the wind field is symmetric around the storm center, whereas when the TC translates in the Northern (Southern) Hemisphere the field is asymmetric, with stronger horizontal and vertical winds right front (left front) of the storm. The model does not resolve rainbands, local convection and turbulent phenomena and therefore produces smooth wind fields.

[6] *Langousis and Veneziano* [2009] extended the MS model to predict TC rain, assuming that the upward moisture flux at the top of the TC boundary layer is all converted into rainfall. The vertical moisture flux is evaluated from the vertical winds generated by the MS model and two additional parameters: the average temperature  $\bar{T}$  and average saturation ratio  $\bar{Q}$  inside the TC boundary layer. We call this the modified-Smith-for-rainfall (MSR) model. The MSR model should prove useful for climatologic studies, but for hazard analysis it has the limitation of ignoring the interstorm and intrastorm variations of rainfall intensity. These variations are highly significant for the assessment of risk. For example, *Lonfat et al.* [2004] found that, also within a given TC strength category, the average of the positive rainfall intensity inside annular regions of 10 km width may deviate from the median value by more than 1 order of magnitude.

[7] Our main objectives are: (1) Extend the MSR model to obtain the probability distribution of the maximum rainfall intensity in an averaging time interval of given duration  $D$  at a fixed geographical location during the passage of a tropical cyclone with given characteristics  $\theta$ , and (2) combine this maximum rainfall model with a TC recurrence model to quantify rainfall risk in the form of intensity-duration-frequency (IDF) curves. For the first objective, we consider a site A at some distance  $y$  to the right ( $y < 0$ ) or left ( $y > 0$ ) of the moving TC center, as shown in Figure 1. As the storm passes, the rainfall intensity

at A fluctuates as a random process  $I(t)$ . Our interest is in  $I_D(t)$ , the moving average of  $I(t)$  for an averaging duration  $D$ , and more specifically in the distribution of  $I_{D,\max}(y, \theta)$ , the maximum of  $I_D(t)$  during the storm.

[8] Section 2 presents our general approach to calculate the distribution of  $I_{D,\max}(y, \theta)$ . This distribution is obtained in section 3 and validated in section 4. Section 4 also shows how the distribution depends on various storm characteristics, the standardized distance  $y/R_{\max}$  from the center of the storm, and the averaging duration  $D$ . Section 5 uses the model of  $I_{D,\max}(y, \theta)$  and a recurrence relation for hurricanes in the Gulf of Mexico to obtain IDF curves for New Orleans and compares these curves with published IDF values for all rainstorms (TCs and non-TCs) combined. Conclusions are stated in section 6.

## 2. A Framework for the Estimation of Extreme TC Rainfall

[9] Our first objective is to relate the distribution of the maximum rainfall intensity  $I_{D,\max}(y, \theta)$  to the smooth rainfall intensities produced by the MSR model of *Langousis and Veneziano* [2009]. The storm parameters are  $\theta = [V_{\max}, R_{\max}, V_t]$ . The analysis uses a Cartesian reference frame  $(x, y)$ , translated and rotated such that the center of the storm O moves to the right along the  $x$  axis; see Figure 1. In this reference, the ordinate  $y$  of A is also the closest (signed) distance of A from the storm center.

[10] To estimate this relationship, we use precipitation radar (PR) data from the TRMM mission [*Simpson et al.*, 1988; *Kummerow et al.*, 1998; *Lee et al.*, 2002]. These data are in the form of swaths about 200 km wide with a spatial resolution of approximately 5 km and have been validated against ground-based radar and rain gauge measurements [*Bolen and Chandrasekar*, 2000; *Liao et al.*, 2001; *Wolff et al.*, 2005]. Due to their long interframe time (about 12 h), the PR snapshots cannot be interpolated to produce the rainfall intensities in continuous time that are needed to estimate rainfall maxima. A common way to overcome this limitation is to use Taylor's frozen turbulence hypothesis [*Taylor*, 1921, 1938]. Under this hypothesis, the temporal variability of rainfall at a fixed location A is statistically the same as the variability that results from translating the frozen-in-time rainfield over A with the storm velocity  $V_t$ . For example, *Vicente et al.* [1998], *Scofield and Kuligowski* [2003], *Kidder et al.* [2005], and *Ferraro et al.* [2005] used Taylor's hypothesis to obtain rainfall totals at fixed locations from satellite and radar rainfall snapshots.

[11] It follows from Taylor's hypothesis that  $I_{D,\max}(y, \theta)$  has the same distribution as  $I_{l,\max}(y, \theta)$ , the maximum of the rainfall intensity averaged in a spatial window of length  $l$  along cross-section C in Figure 1, for  $l = DV_t$ . As an example, Figure 2 shows moving-average rainfall intensities from Hurricane Katrina (2005) along a cross section at distance  $y = 100$  km from the storm center, for averaging lengths  $l = 6$  km (dashed line) and  $l = 24$  km (solid line). The cross section extends over  $L = 384$  km and is symmetric relative to the storm center.

[12] The intensity labeled  $I_L$  in Figure 2 is the average PR rainrate in  $L$ , whereas  $I_{L,MSR}$  is the estimate of that average rainrate produced by the MSR model. These average intensities play an important role in our analysis. For any

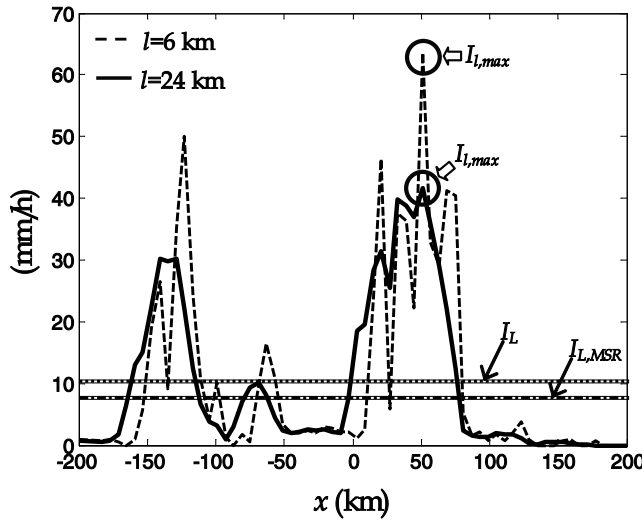


**Figure 2.** Rainfall intensities from Hurricane Katrina (28 August 2005, at 0300 UTC; TRMM frame 44361) along a cross-section C at distance  $y = 100$  km from the storm center, for spatial averaging scales  $l = 6$  and  $24$  km. The maximum values  $I_{l,max}$  are indicated by circles.  $I_L$  is the average value for the entire cross section, and  $I_{L,MSR}$  is the estimate of  $I_L$  produced by the MSR model.

given  $(y, \theta)$  combination, the model estimate  $I_{L,MSR}$  is fixed, whereas  $I_L$  is regarded as a random variable with different values for different tropical cyclones. We model this storm-to-storm variability by expressing  $I_L(y, \theta)$  as

$$I_L(y, \theta) = I_{L,MSR}(y, \theta) \beta_L(y, \theta) \quad (1)$$

where  $\beta_L$  is a random variable.

[13] Figure 2 also shows significant amplification of the rainfall intensity when one considers the maximum over lengths  $l < L$ . One may express the maximum in  $l$ ,  $I_{l,max}$ , as

$$\begin{aligned} I_{l,max}(y, \theta) &= I_{L,MSR}(y, \theta) \beta_{l,max}(y, \theta) \\ &= I_{L,MSR}(y, \theta) \beta_L(y, \theta) \gamma_{l,max}(y, \theta) \end{aligned} \quad (2)$$

where the total factor relative to  $I_{L,MSR}$ ,  $\beta_{l,max}$ , is the product of  $\beta_L$  in equation (1) and a random amplification factor  $\gamma_{l,max}$  for the change of scale from  $L$  to  $l$ . The next section uses PR/TRMM data from 8 tropical cyclones (a total of 38 frames) to derive the distributions of  $\beta_L$  and  $\gamma_{l,max}$ . The selected frames (see Table 1) cover a wide range of TC intensities, from tropical storms to CAT5 systems, under prelandfall conditions. This makes our model best suited for open water sites, but it should also be accurate in coastal areas with a flat topography. For example, *Marks et al.* [2002] [see also *Tuleya et al.*, 2007] used TMI rainfall products for TCs over water to predict rainfall rates at inland locations. For sites close to the shore, the predictions had low bias relative to rain gauge measurements.

[14] Due to the limited lateral coverage of the PR instrument, an additional requirement for selecting the frames was to cover regions close to the hurricane core (with radial

distance less than 300 km from the storm center), as these are the regions that are most critical for rainfall.

### 3. Distribution of $\beta_L$ and $\gamma_{l,max}$

[15] Equation (2) relates the maximum rainfall intensity in  $l$  to the average intensity in  $L$  produced by the MSR model using two random factors: a factor  $\beta_L$  to obtain the average rainfall in  $L$ , and a factor  $\gamma_{l,max}$  to obtain the maximum average intensity at a smaller-scale  $l$ . Sections 3.1 and 3.2 obtain the distribution of these factors using the rainfall information in Table 1 and MSR model simulations.

#### 3.1. Distribution of $\beta_L$

[16] The factor  $\beta_L$  is given by

$$\beta_L(y, \theta) = \frac{I_L(y, \theta)}{I_{L,MSR}(y, \theta)} \quad (3)$$

where  $I_L$  and  $I_{L,MSR}$  are the same as in equation (1). The distribution of  $\beta_L$  generally depends on the distance  $y$  from the TC center and the vector  $\theta = [V_{max}, R_{max}, V_t]$  of storm characteristics, but as we show next, a simple parameterization in terms of the standardized distance  $y' = |y/R_{max}|$  and the large-scale MSR rainfall intensity  $I_{L,MSR}$  suffices. Of course,  $I_{L,MSR}$  is itself a function of  $\theta$ .

[17] Figure 3 shows statistics of  $\beta_L$  as a function of  $y'$  and  $I_{L,MSR}$  for the TRMM frames in Table 1. For each frame, the  $I_{L,MSR}$  intensities at different distances  $y$  from the center of the storm were calculated using the MSR model and the values of  $V_{max}$ ,  $R_{max}$ , and  $V_t$  in the extended best track record [Demuth et al., 2006; M. DeMaria, personal communication, 2008]; see Table 1. In addition to  $V_{max}$ ,  $R_{max}$ , and  $V_t$ , the MSR model requires specification of the vertical diffusion coefficient  $K$ , the surface drag coefficient  $C_d$ , the vertically averaged temperature  $\bar{T}$  and saturation ratio  $\bar{Q}$  inside the boundary layer (BL), Holland's  $B$  parameter for the profile of gradient winds, the sloping angle  $\psi_0$  and height  $H_0$  of the wall updraft, and the temporal scale  $t_r$  for azimuthal redistribution of rainfall by the cyclonic circulation; see *Langousis and Veneziano* [2009] for details. In our simulations we have set  $K = 50$  m<sup>2</sup>/s,  $C_d = 0.002$ ,  $\bar{T} = 22^\circ\text{C}$ ,  $\bar{Q} = 0.8$ ,  $B = 1$ ,  $\psi_0 = 50^\circ$ ,  $H_0 = 6$  km and  $t_r = 60$  min. *Langousis and Veneziano* [2009] recommend these settings as representative of tropical cyclones in the North Atlantic and as values that reproduce well the TRMM/PR rainfall fields in an ensemble-average sense.

[18] Figures 3a and 3b show smooth contour plots of the log mean  $m_{\ln\beta_L}$  and log standard deviation  $\sigma_{\ln\beta_L}$  of  $\beta_L$  as a function of the standardized distance  $y' = |y/R_{max}|$  and the MSR rainfall intensity  $I_{L,MSR}$  for the 38 frames in Table 1. For each frame, a regular spacing  $\Delta y = 10$  km was maintained between adjacent transects, producing a total of 789 points; see Figure 3a. In all cases, averaging is over segments of length  $L = 384$  km, symmetric relative to the storm center. This value of  $L$  encompasses more than 95% of the total rainfall volume along each transect; see for example Figure 2. Smooth estimates of the mean value and variance of  $\ln\beta_L$  were obtained using an isotropic Gaussian kernel with standard deviation 0.5 in the  $[\ln(I_{L,MSR}), \ln(y')]$  plane. Hence, if  $g(\mathbf{x})$  denotes this kernel, local estimates of

**Table 1.** Characteristics of the PR/TRMM Rain Frames Used in the Analysis<sup>a</sup>

	Storm Center		Storm Speed (m/s)	Storm Direction (deg)	$V_{\max}$ (m/s)	$R_{\max}$ (km)	TRMM Frame	Storm Intensity	
	Latitude (deg)	Longitude (deg)							
Floyd 1999	21.7	-61.6	4.9	143	48.8	41	10290	CAT2	
	23.5	-68.7	4.8	169	64.0	37	10317	CAT4	
	23.7	-70.6	5.8	171	69.3	37	10321	CAT4	
Frances 2004	12.6	-43.7	10.9	158	23.1	37	38646	TS	
	15.7	-49.8	5.4	139	51.4	19	38667	CAT3	
	17	-51.3	5.3	139	54.0	28	38677	CAT3	
	17.9	-52.6	4.3	144	59.1	28	38682	CAT4	
	19	-57.3	4.9	180	51.4	28	38708	CAT3	
	21.2	-68.5	6.1	162	61.7	28	38739	CAT4	
Ivan 2004	8.9	-38.9	7.6	184	25.7	37	38789	TS	
	10.7	-50.6	12.2	185	57.5	28	38814	CAT4	
	11.2	-53.4	8.1	173	51.4	28	38820	CAT3	
	12.3	-64.1	8.3	166	61.7	19	38845	CAT4	
	12.7	-66.2	7.3	164	61.7	20	38851	CAT4	
	17.4	-77.3	4.1	194	66.8	28	38892	CAT4	
	17.7	-78.4	4.4	153	64.3	28	38897	CAT4	
	25.6	-87.4	5.5	112	61.7	46	38954	CAT4	
	27.4	-70.6	5.5	0	38.6	42	39045	CAT1	
Jeanne 2004	25.5	-69.5	1.1	207	41.1	37	39079	CAT2	
	26.5	-74.3	7.4	173	43.7	60	39106	CAT2	
	26.5	-75.6	6.5	180	46.3	46	39110	CAT2	
	Karl 2004	11.5	-35.3	7.1	176	26.7	37	38987	TS
	17.3	-45.5	2.0	166	57.8	32	39033	CAT3	
Katrina 2005	19.1	-47.4	5.9	121	64.0	32	39048	CAT4	
	22.9	-48.6	8.2	112	54.0	28	39059	CAT3	
	25.7	-49.5	6.8	117	48.8	28	39063	CAT3	
	24.6	-85.6	2.1	153	51.5	56	44357	CAT3	
	25	-86.2	3.5	146	56.5	50	44361	CAT3	
	26.9	-89	5.5	135	75.0	38	44373	CAT5	
Lilli 2002	23.6	-87.2	9.0	162	51.5	20	27826	CAT2	
	24.4	-88.4	6.2	141	56.5	20	27830	CAT2	
	28.4	-91.4	10.1	117	54.0	20	27842	CAT4	
	29	-91.9	5.4	124	41.1	20	27845	CAT2	
Rita 2005	24.3	-85.9	5.7	189	61.7	28	44743	CAT4	
	24.9	-88	3.9	166	77.1	19	44754	CAT5	
	25.4	-88.7	4.3	153	72.0	19	44758	CAT5	
	26.8	-91	5.5	135	59.1	37	44770	CAT4	
	27.4	-91.9	4.8	143	59.1	37	44773	CAT4	

<sup>a</sup>The direction of storm translation is relative to the east and is positive counterclockwise. The estimates of  $V_{\max}$  and  $R_{\max}$  are from the extended best track record (M. DeMaria, personal communication, 2008).

$m_{\ln\beta_L}(\mathbf{x}_0)$  and  $\sigma_{\ln\beta_L}^2(\mathbf{x}_0)$  around a given point  $\mathbf{x}_0 = [\ln(I_{L,MSR}), \ln(y')]$  are given by

$$m_{\ln\beta_L}(\mathbf{x}_0) = \frac{\sum_i \ln\beta_L(\mathbf{x}_i)g(\mathbf{x}_i - \mathbf{x}_0)}{\sum_i g(\mathbf{x}_i - \mathbf{x}_0)},$$

$$\sigma_{\ln\beta_L}^2(\mathbf{x}_0) = \frac{\sum_i [\ln\beta_L(\mathbf{x}_i) - m_{\ln\beta_L}(\mathbf{x}_0)]^2 g(\mathbf{x}_i - \mathbf{x}_0)}{\sum_i g(\mathbf{x}_i - \mathbf{x}_0)} \quad (4)$$

where  $\mathbf{x}_i$  is the generic  $[\ln(I_{L,MSR}), \ln(y')]$  combination for which a value of  $\beta_L$  is available. To use values of  $\beta_L$  at locations close to the center of the storm where  $\ln(y')$  diverges, 59 points with  $|y'| < 0.5 R_{\max}$  where moved to  $y = 0.5 R_{\max}$ .

[19] The overall mean value of  $\beta_L$  is 1.02, indicating that on average the MSR model produces unbiased large-scale estimates of the PR rainrates. The dashed lines in Figure 3b delimit the region of high data density and are generally oriented along the gradient of  $\sigma_{\ln\beta_L}$ . Figure 3c shows plots of  $m_{\ln\beta_L}$  and  $\sigma_{\ln\beta_L}$  as a function of the transformed variable  $\omega = \ln(y') - 0.4\ln(I_{L,MSR})$  along the dashed-dotted line in

Figure 3b. The log mean  $m_{\ln\beta_L}$  is approximately constant and equal to  $-0.5$ , whereas  $\sigma_{\ln\beta_L}$  increases as the standardized distance  $y'$  increases or the large-scale mean rainfall intensity  $I_{L,MSR}$  decreases. This higher log variability in regions of lower intensity is expected due to the more episodic nature of rainfall in those regions. This is also in qualitative agreement with the findings of *Lonfat et al.* [2004] and *Molinari et al.* [1994]. The solid lines in Figure 3c are least squares fits for the mean and standard deviation of  $\ln\beta_L$ . For  $y$  close to zero, the fitted standard deviation becomes very small or negative. To avoid this inconsistency, we have imposed a lower bound of 0.5 to the fitted standard deviation.

[20] To investigate the distribution type, we standardize the empirical values of  $\ln\beta_L$  by removing the parametrically fitted mean  $-0.5$  and dividing by the parametrically fitted standard deviation  $0.25\omega + 0.87$ . Figure 3d shows a histogram of these standardized quantities and suggests that  $\ln\beta_L$  has near-normal distribution. To check for possible lack of fit and possible dependence of  $\ln\beta_L$  on other parameters, we generated histograms of the type in Figure 3d separately for different ranges of  $y$ ,  $I_{L,MSR}$ ,  $R_{\max}$  and  $V_{\max}$  [see *Langousis,*

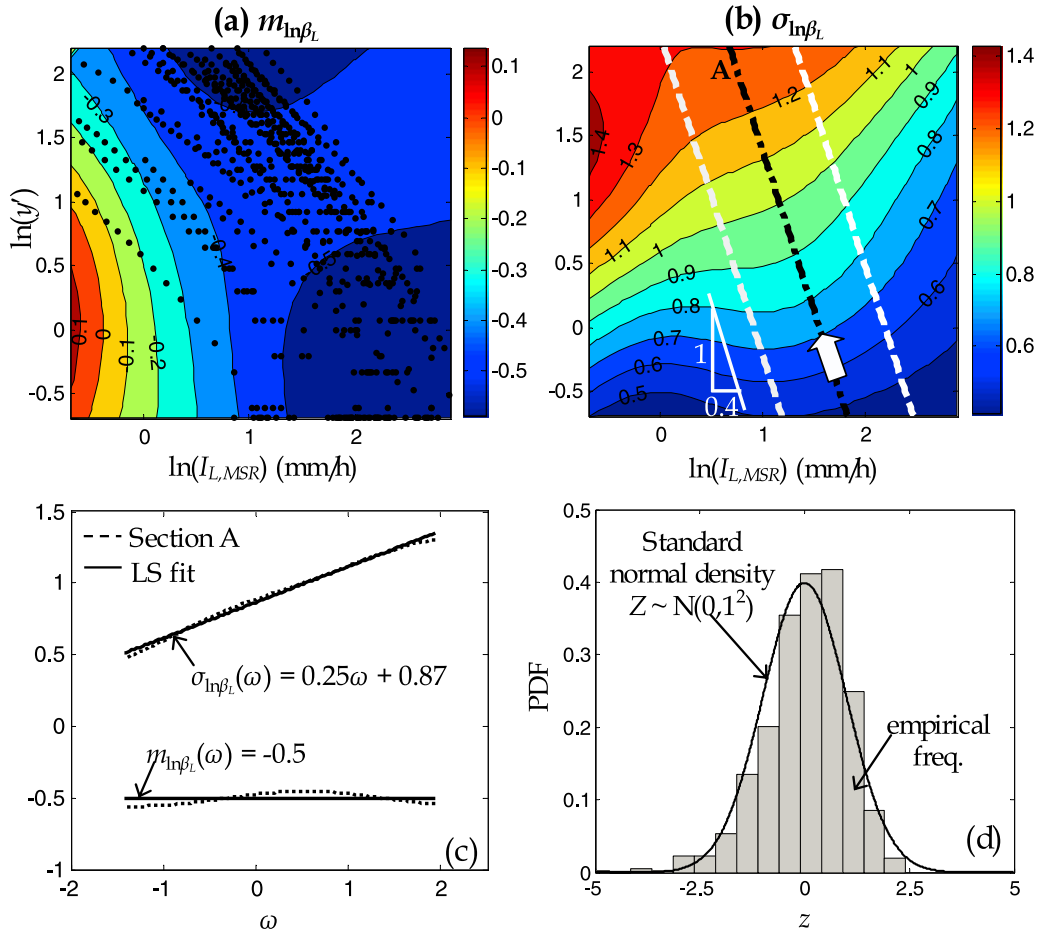


**Figure 3.** (a, b) Mean value and standard deviation of  $\ln\beta_L$  as a function of the model rainfall intensity  $I_{L,MSR}$  and the standardized distance  $y' = |y/R_{\max}|$  from the TC center using 789 cross sections of the 38 frames in Table 1. The contour plots are obtained using a smoothing Gaussian kernel with standard deviation 0.5. The dashed lines delimit the region of high data density along the direction of the gradient of  $\sigma_{\ln\beta_L}$  (white arrow). (c) Plots of  $m_{\ln\beta_L}$  and  $\sigma_{\ln\beta_L}$  as a function of  $\omega = \ln(y') - 0.4\ln(I_{L,MSR})$  along cross-section A. (d) Comparison between the standard normal density and the empirical PDF of  $\ln\beta_L$ , standardized to have zero mean and unit variance.

2008]. As none of these analyses reveals significant dependence, we use the fits in Figure 3c and model  $\ln\beta_L$  as a normal variable with parameters

$$\begin{aligned} m_{\ln\beta_L}(\omega) &= -0.5 \\ \sigma_{\ln\beta_L}(\omega) &= \max\{0.5, 0.25\omega + 0.87\} \end{aligned} \quad (5)$$

where  $\omega = \ln(y') - 0.4\ln(I_{L,MSR})$ .

### 3.2. Distribution of $\gamma_{l,\max}$

[21] Next we consider the amplification factor  $\gamma_{l,\max}$  in equation (2). The distribution of this factor can be found by a variety of methods, from the direct use of data on  $\gamma_{l,\max}$  from the frames in Table 1 to theoretical analysis of the maximum of the moving-average processes  $I_l(x)$  illustrated in Figure 2. Langousis [2008] compared several such approaches and found similar results. Here we follow the empirical approach, which is the simpler and more transparent method. We start by calculating the empirical ratio

$$\gamma_{l,\max} = \frac{I_{l,\max}}{I_l}, \quad l \leq L \quad (6)$$

where  $I_l$  is the average PR rainrate along a cross-section C of fixed length  $L = 384$  km and  $I_{l,\max}$  is the maximum rainfall intensity when the same cross section is continuously scanned using an averaging window of length  $l$ ; see Figures 1 and 2 and section 2. Ideally, the cross-section C should be in the direction of the storm motion, but since the TRMM swaths are not always aligned with that direction, we calculate the factor  $\gamma_{l,\max}$  using cross sections parallel to the swath track. Hence, the resulting factor  $\gamma_{l,\max}$  does not depend on the orientation of C relative to the storm motion. Langousis [2008] verified that  $\gamma_{l,\max}$  is insensitive to this orientation by dividing the swaths into two groups: those that are generally aligned with the storm trajectory and those that are not. The distribution of  $\gamma_{l,\max}$  is similar in the two cases.

[22] Langousis [2008] also studied the dependence of the distribution of  $\gamma_{l,\max}$  on  $R_{\max}$ . Dependence is expected because smaller values of  $R_{\max}$  produce more peaked radial rainfall profiles and hence higher rainfall maxima. The finding is that for small spatial scales ( $l \leq 12$  km) the mean value and standard deviation of  $\gamma_{l,\max}$  increase somewhat with decreasing  $R_{\max}$ , whereas at larger spatial scales the

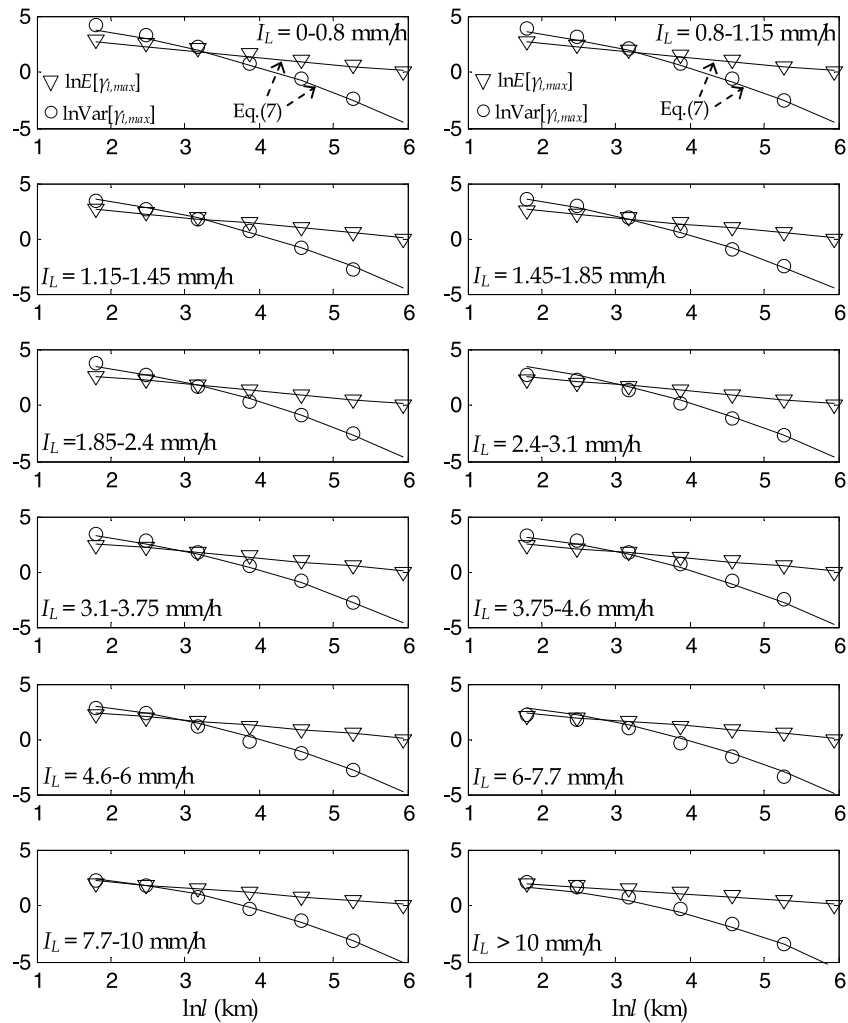


**Figure 4.** Log-log plots of  $E[\gamma_{l,\max}]$  and  $\text{Var}[\gamma_{l,\max}]$  against  $l$  for different ranges of  $I_L$ . Triangles and circles indicate empirical values. The solid lines are from equations (7a) and (7b).

increase is modest. Based on these results, we ignore the dependence of  $\gamma_{l,\max}$  on  $R_{\max}$  and use a simple parameterization in terms of the averaging length  $l$  and the large-scale average intensity  $I_L$ . The latter quantity depends significantly on both the storm intensity  $V_{\max}$  and the distance  $y$  from the storm center [see *Langousis and Veneziano, 2009*].

[23] Figure 4 shows log-log plots of  $E[\gamma_{l,\max}]$  and  $\text{Var}[\gamma_{l,\max}]$  against  $l$  after classifying the 789 cross sections in Figure 3a into 12 equally sized  $I_L$  bins. As expected,  $\text{Var}[\gamma_{l,\max}]$  increases with decreasing spatial scale  $l$ . A less obvious finding is that the variability of  $\gamma_{l,\max}$  increases as the large-scale intensity  $I_L$  decreases. Considering that lower values of  $I_L$  are generally found at larger distances  $y$  from the storm center, Figure 4 shows that the outer TC environment exhibits higher (multiplicative) variability relative to the inner region. The higher variability inside low- $I_L$  regions is due for the most part to an increase in the dry area fraction [*Langousis, 2008*] and has been noted also in other studies [*Molinari et al., 1994; Lonfat et al., 2004*]. This feature is also commonly observed in extratropical rainfall [e.g., *Over and Gupta, 1996; Deidda et al., 2006; Veneziano et al., 2006a; Gebremichael et al., 2006*].

[24] For each intensity category  $I_L$ , we use least squares to fit linear and quadratic expressions for the log mean and log variance of  $\gamma_{l,\max}$ ,

$$\ln E[\gamma_{l,\max}] = \alpha_1 \ln l + \alpha_2 \quad (7a)$$

$$\ln \text{Var}[\gamma_{l,\max}] = \alpha_3 (\ln l)^2 + \alpha_4 \ln l + \alpha_5 \quad (7b)$$

where  $l \leq L$  is in km and  $a_1 - a_5$  are parameters. Figure 5 shows how the parameters  $a_1 - a_5$  in equations (7a) and (7b) vary with the large-scale rainfall intensity  $I_L$ . The solid lines in Figure 5 are smooth least squares estimates of  $a_i$  ( $i = 1, \dots, 5$ ). Use of the smooth estimates reproduces well the empirical moments of  $\gamma_{l,\max}$ ; see solid lines in Figure 4.

[25] The amplification factor  $\gamma_{l,\max}$  has values between 1 and  $L/l$ . The lower bound corresponds to a uniform distribution of rainfall inside  $L$ , whereas the upper bound is attained when all the rainfall in  $L$  is concentrated in a single

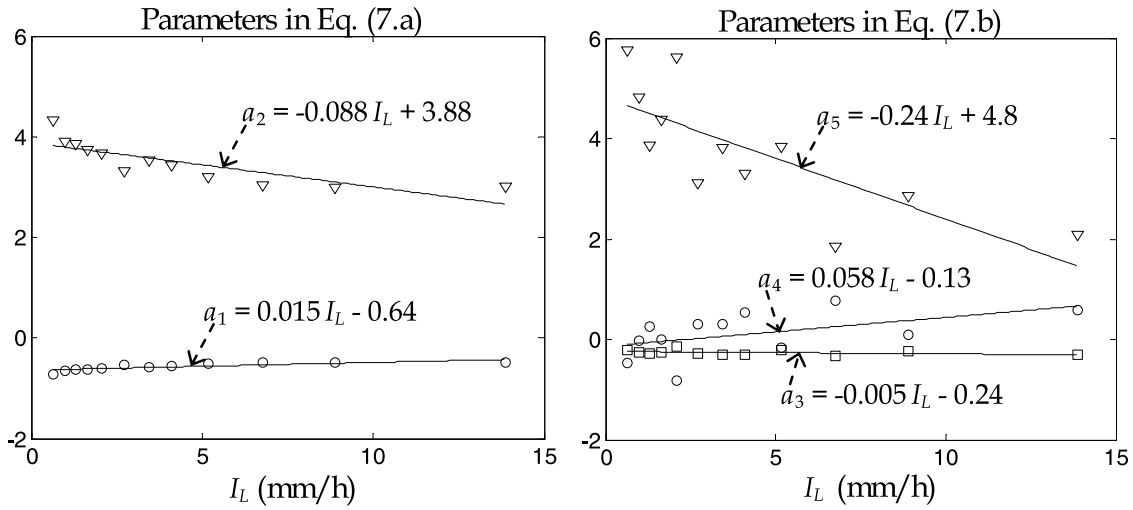


**Figure 5.** Dependence of the parameters  $a_1 - a_5$  in equations (7a) and (7b) on  $I_L$ . The solid lines are least squares fits.

$l$  interval. We model  $\gamma_{l,\max}$  using a beta distribution with moments in equations (7a) and (7b). One may write this cumulative distribution as

$$F_{\gamma_{l,\max}}(\gamma) = F_X\left(\frac{\gamma-1}{L/l-1}\right), \quad \gamma \geq 1 \quad (8)$$

where  $F_X$  is the beta distribution in  $[0, 1]$  with parameters

$$E[X] = \frac{E[\gamma_{l,\max}] - 1}{L/l - 1}, \quad \text{Var}[X] = \frac{\text{Var}[\gamma_{l,\max}]}{(L/l - 1)^2} \quad (9)$$

Figure 6 compares the empirical distribution of  $\gamma_{l,\max}$  at spatial scales  $l=96$  and  $6$  km for different large-scale average intensities  $I_L$  with theoretical distributions from equations (8) and (9). The moments  $E[\gamma_{l,\max}]$  and  $\text{Var}[\gamma_{l,\max}]$  in equation (9) are calculated using equations (7a) and (7b) with parameters  $a_1 - a_5$  in Figure 5. Equally good fits are obtained for other window sizes  $l$  [see Langousis, 2008].

#### 4. Validation of Maximum Rainfall Model and Sensitivity Analysis

[26] For a tropical cyclone with parameters  $\theta = [V_{\max}, R_{\max}, V_t]$  and a given distance  $y$  from the storm center, one may use equation (2) and the distributions of  $\beta_L$  and  $\gamma_{l,\max}$  in section 3 to obtain the distribution of the maximum rainfall intensity  $I_{l,\max}$  as

$$P[I_{l,\max}(y, \theta) \leq i] = \int_0^{\infty} f_{I_L|y,\theta}(u) F_{\gamma_{l,\max}|I_L=u}(i/u) du \quad (10)$$

where  $f_{I_L|y,\theta}$  is the probability density function of  $I_L = I_{L,MSR}$   $\beta_L$  given  $(y, \theta)$  and  $F_{\gamma_{l,\max}|I_L}$  is the cumulative distribution function of  $\gamma_{l,\max}$  given  $I_L$ . To assess the validity of the probabilities generated by equation (10), we compare them with observed relative frequencies, as follows. For each of the 789 transects extracted from the PR data in Table 1, we perform the following steps:

[27] 1. We calculate the maximum intensity  $I_{l,\max}$  over segments of different length  $l$ .

[28] 2. We use  $(V_{\max}, R_{\max}, V_t)$  from Table 1 and the distance  $y$  of the transect from the TC center to obtain model estimates of the large-scale mean rainfall intensity  $I_{L,MSR}(y, \theta)$  for  $L = 384$  km. All other MSR model parameters are fixed to the values in section 3.1.

[29] 3. We use equation (10) and the parametric expressions in equations (5) and (7a–7b) and Figure 5 to find the distribution of  $I_{l,\max}$  and the probability  $P$  with which the observed value from step 1 is not exceeded.

[30] If the model is correct, the probabilities  $P$  from step 3 have uniform distribution between 0 and 1. Figure 7 shows histograms of  $P$  for different  $l$ . One sees that the histograms differ somewhat from a uniform density (the chi-square goodness of fit test applied to the bins shown in Figure 7 passes at a level of significance around 0.005–0.01 depending on the scale of averaging  $l$ ). We have investigated this issue in some detail [Langousis, 2008] and found that the biases are due mainly to dependence of the amplification factor  $\gamma_{l,\max}$  on the radius of maximum winds  $R_{\max}$ ; see section 3.2. Although a parameterization of  $\gamma_{l,\max}$  that includes  $R_{\max}$  as an independent variable would improve the goodness of fit, here we retain the simpler model.

[31] The distribution of  $I_{l,\max}$  in equation (10) depends critically on the amplification factor  $\beta_{l,\max}$  in equation (2). Figure 8 shows how the distribution of  $\beta_{l,\max}$  depends on  $l$ ,  $V_{\max}$ , and  $y' = |y/R_{\max}|$ . The effect of the translation velocity  $V_t$  is modest and is not displayed. Also, for given  $V_{\max}$  and  $y' = |y/R_{\max}|$ ,  $\beta_{l,\max}$  is insensitive to  $R_{\max}$ . The dispersion of  $\beta_{l,\max}$  increases as  $l$  decreases. It also increases for smaller  $V_{\max}$  and larger  $y'$ . The latter effects are related to the increased spatial variability of the rainfall intensity in regions of lower average precipitation.

#### 5. Long-Term Rainfall Risk for New Orleans

[32] To assess rainfall risk at a given location A, one must find the rate  $\lambda_{I_{D,\max} > i}$  of tropical cyclones for which  $I_{D,\max}$ , the maximum rainfall intensity at A for a given averaging

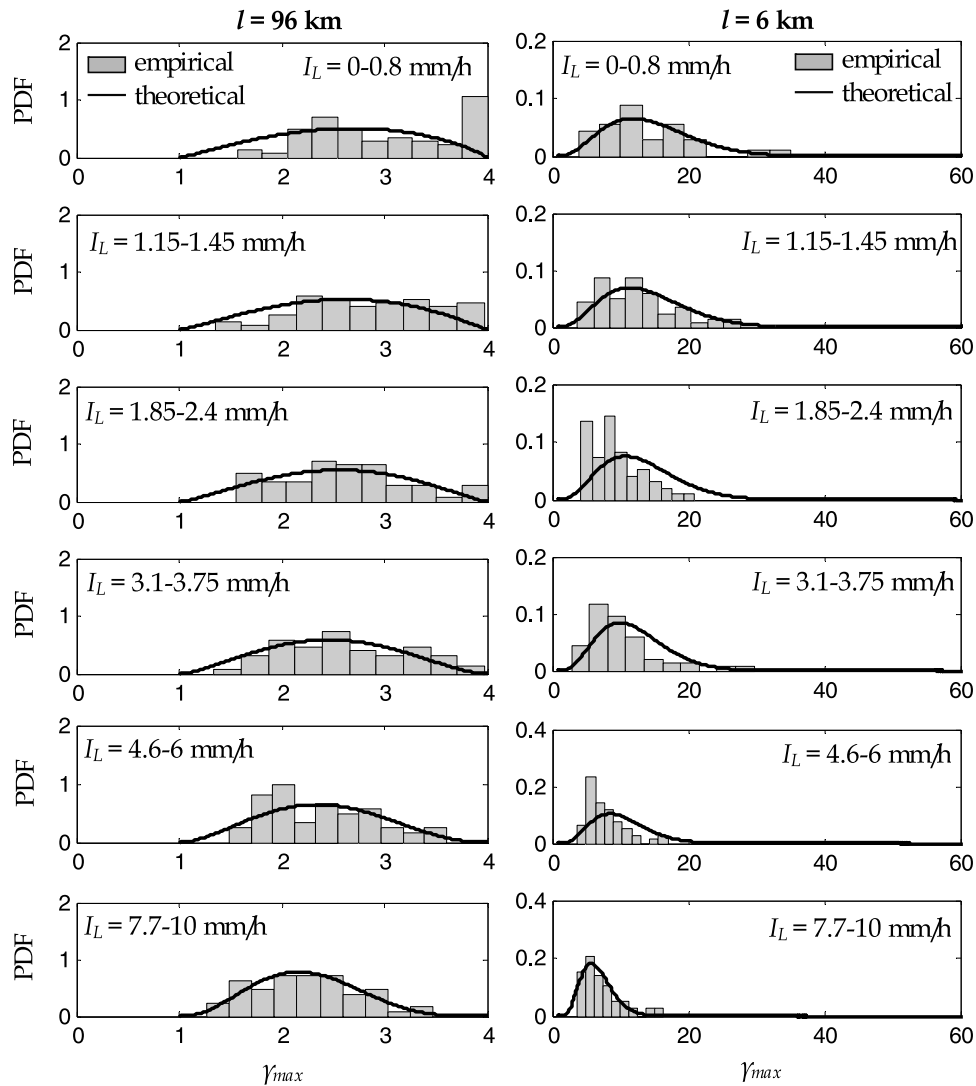


**Figure 6.** Comparison of histograms of  $\gamma_{l,max}$  for  $l = 96$  and  $6$  km and different large-scale intensities with theoretical distributions from equations (7a), (7b), and (8). The intensity categories are the same as in Figure 4 (left).

duration  $D$ , exceeds different threshold levels  $i$ . This rate is given by

$$\begin{aligned} \lambda_{I_{D,max} > i} &= \lambda P[I_{D,max} > i] \\ &= \lambda \int_{\text{all}(y,\theta)} P[I_{D,max}(y, \theta) > i] f_{y,\theta}(y, \theta) dy d\theta \end{aligned} \quad (11)$$

where  $\lambda$  is the rate of TCs in the region,  $P[I_{D,max}(y, \theta) > i]$  is the probability that, for a storm with characteristics  $\theta$ ,  $I_{D,max}$  at distance  $y$  from the storm center exceeds  $i$ , and  $f_{y,\theta}$  is the joint density of  $(y, \theta)$ . The joint density  $f_{y,\theta}$  and the rate  $\lambda$  are region-specific and define the TC recurrence model. Under Taylor’s hypothesis,  $P[I_{D,max}(y, \theta) > i]$  is obtained by setting  $l = DV_i$  in equation (10).

[33] To exemplify, we use equation (11) and a recurrence model for an appropriate coastal region of the Gulf of Mexico to obtain intensity-duration-frequency (IDF) relationships for New Orleans. We select this location because:

- (1) the site is close to the coast and has a flat topography; hence our prelandfall model should produce accurate results,
- (2) a number of studies have developed TC recurrence models for the Louisiana coast, and
- (3) one can compare the TC rainfall results with available IDF curves from continuous rainfall records in the region.

### 5.1. TC Recurrence Model for the Northern Gulf of Mexico

[34] We start by specifying the distribution of the distance  $y$  between the center of the storm and the city of New Orleans (point A), which is located at approximately  $(90^\circ\text{W}, 30^\circ\text{N})$ . Then we consider the distribution of  $\theta = [V_{max}, R_{max}, V_i]$ . The joint model for  $V_{max}$  and  $R_{max}$  is specified through the distribution of the maximum pressure deficit  $\Delta P_{max}$  and the conditional distributions of  $[V_{max}|\Delta P_{max}]$  and  $[R_{max}|\Delta P_{max}]$ . Finally we specify the TC rate  $\lambda$ . To keep the model simple, we approximate the coastline by a line segment with constant latitude  $30^\circ\text{N}$  and longitudinal range  $85^\circ-95^\circ\text{W}$  ( $\approx 960$  km), centered at A.

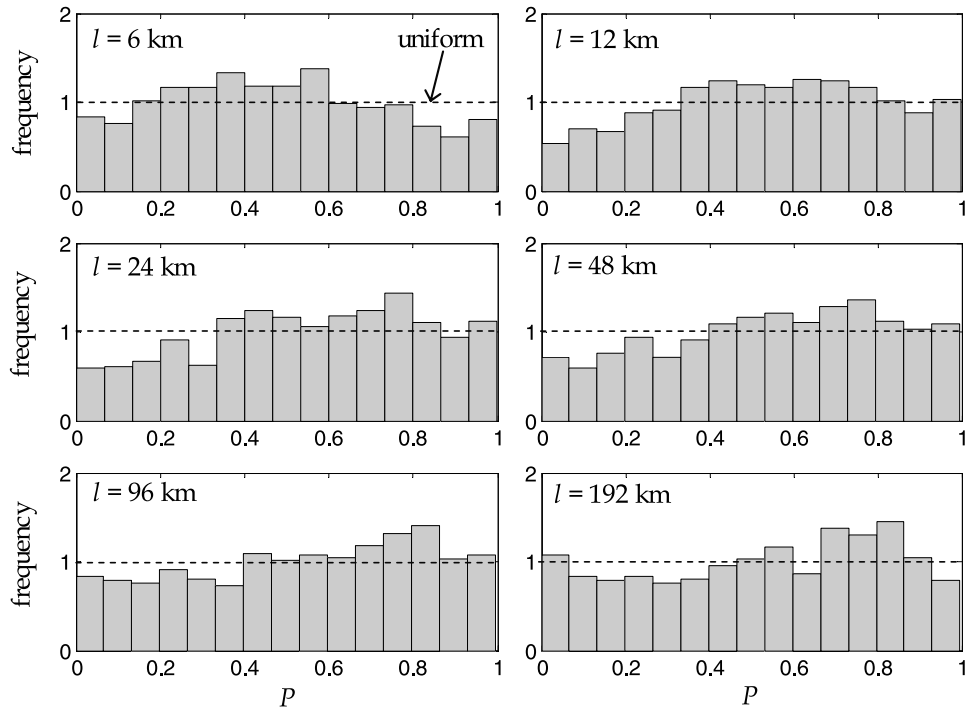


**Figure 7.** Histogram of the nonexceedance probability  $P$  in equation (10) for different spatial scales  $l$ . Each histogram is based on a sample of size 789.

[35] Let  $z$  be the location (positive eastward) of landfall relative to A. Assuming a straight storm path, the closest distance of the storm center from the site is

$$y = -z \cos(\alpha) \quad (12)$$

where  $\alpha$  is the azimuth of the storm track at landfall, positive clockwise. The distribution of  $y$  can be obtained numerically from equation (12) and the distributions of  $\alpha$  and  $z$ , assumed here to be independent. For  $z$  we use a uniform distribution in the interval  $[85^\circ\text{W}, 95^\circ\text{W}]$ . The distribution of the angle  $\alpha$  in the region is usually found to be normal or the mixture of two normal distributions, one for easterly storms and the other for westerly storms [Vickery and Twisdale, 1995; IPET, 2006, 2008]. Here we model  $\alpha$  using a single normal distribution with mean value  $m_\alpha = -5.4^\circ$  and standard deviation  $\sigma_\alpha = 34.9^\circ$ . This distribution was obtained by IPET [2006] using NOAA's HURDAT data set [Jarvinen et al., 1984] and found to describe well storms with central pressure deficit  $\Delta P_{\max} > 34$  hPa that make landfall in the longitudinal range  $85^\circ - 95^\circ\text{W}$ .

[36] Several studies [Holland, 1980; Atkinson and Holiday, 1977; Willoughby and Rahn, 2004] have used theoretical arguments and pressure-wind observations to relate  $V_{\max}$  to  $\Delta P_{\max}$ . The relationships are typically of the power law type

$$V_{\max} = c(\Delta P_{\max})^g \quad (13)$$

where  $c$  and  $g$  are positive constants. Using flight level data from 23 hurricane seasons, Willoughby and Rahn [2004] found  $c = 4.8$  and  $g = 0.559$  for  $V_{\max}$  in m/s and  $\Delta P_{\max}$  in hPa. Based on these and other findings of Willoughby and Rahn [2004], we model  $[V_{\max}|\Delta P_{\max}]$  as a lognormal

variable with mean value  $4.8(\Delta P_{\max})^{0.559}$  and coefficient of variation 0.15.

[37] Empirical evidence [Vickery and Twisdale, 1995; Vickery et al., 2000; Willoughby and Rahn, 2004; Powell et al., 2005; IPET, 2008] and theoretical arguments [Shen, 2006] show that  $R_{\max}$  increases when the hurricane intensity  $\Delta P_{\max}$  decreases or the latitude  $\phi$  increases. Here we assume that  $(\ln R_{\max}|\Delta P_{\max})$  has the normal distribution proposed by Vickery et al. [2000], which for the region of New Orleans ( $\phi \approx 30^\circ\text{N}$ ) has parameters

$$\begin{aligned} m_{\ln R_{\max}|\Delta P_{\max}} &= 3.962 - 0.00567\Delta P_{\max} \\ \sigma_{\ln R_{\max}|\Delta P_{\max}} &= 0.313 \end{aligned} \quad (14)$$

where  $R_{\max}$  is in km and  $\Delta P_{\max}$  is in hPa.

[38] The translational speed  $V_t$  has weak dependence on the intensity of the TC [Chen et al., 2006; IPET, 2008] and is usually modeled as a lognormal variable with mean value around 6 m/s and standard deviation around 2.5 m/s [see Vickery and Twisdale, 1995; Vickery et al., 2000; Chen et al., 2006]. The former two studies report a slight dependence of  $V_t$  on the approach angle  $\alpha$ . To keep the TC recurrence model simple, we use for  $V_t$  a lognormal distribution with the above mean value and standard deviation and assume that  $V_t$  and  $\alpha$  are independent.

[39] Different studies have concluded that the pressure deficit  $\Delta P_{\max}$  has lognormal, Weibull or Gumbel distribution. The Weibull distribution gives better fits when all tropical cyclones are considered, whereas the lognormal distribution is more appropriate for storms in the hurricane intensity range [see Vickery and Twisdale, 1995; Chouinard et al., 1997; IPET, 2006]. The Gumbel distribution has been suggested by IPET [2008] for storms in the CAT35 range

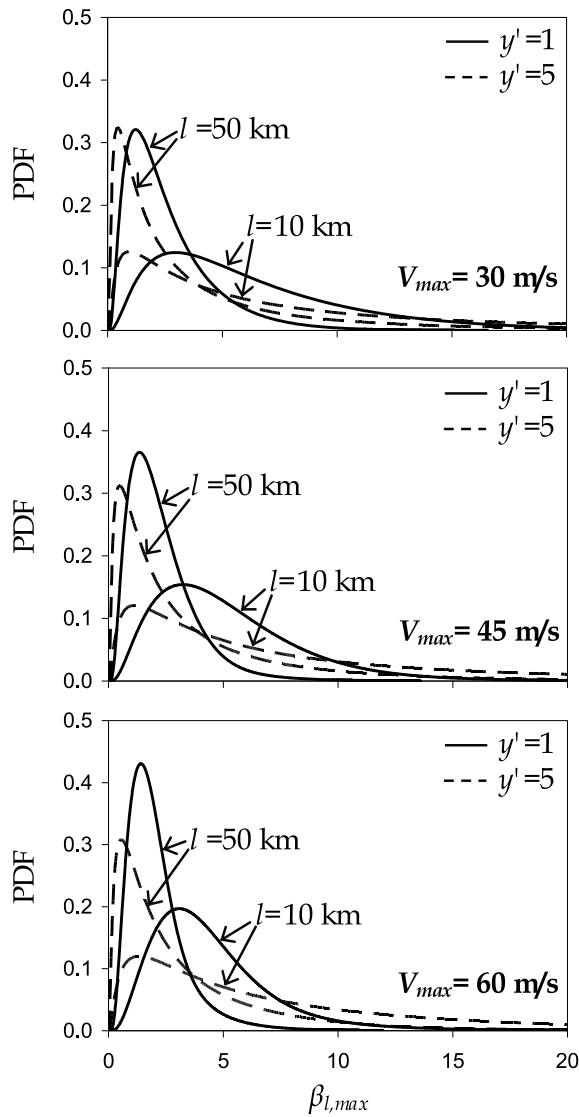


**Figure 8.** Comparison of the probability density functions of  $\beta_{l,\max} = I_{l,\max}/I_{L,MSR}$  for different  $V_{\max}$ ,  $y' = |y/R_{\max}|$ , and  $l$ .

( $\Delta P_{\max} > 58$  hPa). While the Gumbel distribution is appropriate for the analysis of surges, winds and waves (for which the long-term risk is dominated by intense storms), significant rainfall is contributed by less intense slow-moving systems; see section 5.2. For this reason we model  $\Delta P_{\max}$  using the lognormal distribution suggested by *IPET* [2006]. This study shows that for TCs with  $\Delta P_{\max} > 34$  hPa that made landfall in the longitudinal range  $85^\circ$ – $95^\circ$ W,  $\Delta P_{\max}$  is accurately described by a shifted lognormal distribution with shift parameter 18 hPa, log mean 3.15 and log standard deviation 0.68. Finally, we set  $\lambda = 0.57$  events/year, which is the rate found by *IPET* [2006] for TCs with  $\Delta P_{\max} > 34$  hPa making landfall between  $85^\circ$  and  $95^\circ$ W along the Gulf of Mexico coast.

## 5.2. IDF Curves for TC Rainfall and Comparison With Other Storms

[40] Next we use equation (11) with the recurrence model in section 5.1 to estimate the intensity-duration-frequency (IDF) curves for New Orleans associated with tropical

cyclones. The model explicitly accounts for variability in  $y$ ,  $V_{\max}$ ,  $R_{\max}$  and  $V_i$ . All other input parameters to the MSR model are fixed to the values used in sections 3 and 4. The joint density of  $\{y, V_{\max}, R_{\max}, V_i\}$  for a TC that makes landfall between longitudes  $85^\circ$ – $95^\circ$ W,  $f_{y,\theta}$ , is obtained by first calculating the joint density conditional on the pressure deficit  $\Delta P_{\max}$  under the assumption that the variables  $y$ ,  $[V_{\max}|\Delta P_{\max}]$ ,  $[R_{\max}|\Delta P_{\max}]$  and  $V_i$  are independent and then averaging the conditional density with respect to  $\Delta P_{\max}$ .

[41] Figure 9a shows the calculated IDF curves as plots of rainfall intensity  $i$  against the averaging duration  $D$  for different return periods  $T$ . For averaging durations below about 12 h, the decay of  $i$  with  $D$  follows a power law  $D^{-\gamma_D}$  where  $\gamma_D \approx 0.55$ . This exponent is slightly smaller than the values around 0.6–0.7 that are typical of extratropical rainfall (because the rainfall intensities associated with long durations in TCs tend to be high relative to extratropical events) [see, e.g., *Langousis et al.*, 2007]. For longer averaging durations, the exponent  $\gamma_D$  rapidly increases and is effectively 1 for  $D > 24$  h; see dashed lines in Figure 9a. The reason is that the passage of a hurricane usually lasts less than 24 h; hence for  $D > 24$  h the total rainfall depth is approximately constant and the average rainfall intensity depends on  $D$  like  $D^{-1}$ .

[42] Figure 9b shows the same results as plots of  $T$  against  $i$  for different averaging durations  $D$ . To determine the importance of TCs relative to other storm types in rainfall risk, the calculated IDF curves are compared with values from TP-40 [*Hershfield*, 1961], *Babak et al.* [1991], and *Singh and Zhang* [2007] for return periods  $T = 5, 10, 25, 50$ , and 100 years. The latter values refer to generic rainfall in the New Orleans area and therefore include both TC and non-TC events. The rainfall values reported in TP-40 cover the whole range of averaging durations  $D$  from 0.5 to 24 h, whereas *Babak et al.* [1991] and *Singh and Zhang* [2007] give rainfall values only for  $D = 6, 12$  and 24 h. It is clear from Figure 9b that for  $T > 100$  years also the dependence of the rainfall intensity on  $T$  is of the power law type, say  $T^{\gamma_T}$  with  $\gamma_T \approx 0.32$ . This exponent is higher than the values around 0.20–0.25 that are typical of ordinary rainfall [*Langousis et al.*, 2007; *Veneziano et al.*, 2006b]. The higher exponent in tropical cyclones is related to the large dispersion of the amplification factor  $\beta_{l,\max}$  (see example plots in Figure 8).

[43] Another feature of the TC curves in Figure 9b is the lower asymptote at  $T = 1/\lambda = 1.75$  years. This lower bound is a consequence of the fact that the return period of any TC-induced rainfall intensity cannot be lower than the return period of the TCs themselves. The effect of this lower bound is that for short return periods, say  $T < 10$  years, the precipitation intensities from tropical cyclones are far below those from ordinary rainfall (frontal events, mesoscale convective systems, etc.), for which the recurrence rate is much higher. By contrast, for long averaging durations ( $D > 12$  h) and long return periods ( $T = 100$  years), the calculated TC intensities are close to the empirical intensities, indicating that tropical cyclones have a dominant effect on those extreme values. Given that the TC curves in Figure 9b are flatter than those for overall rain, it is expected that tropical cyclones become even more dominant for longer return periods.

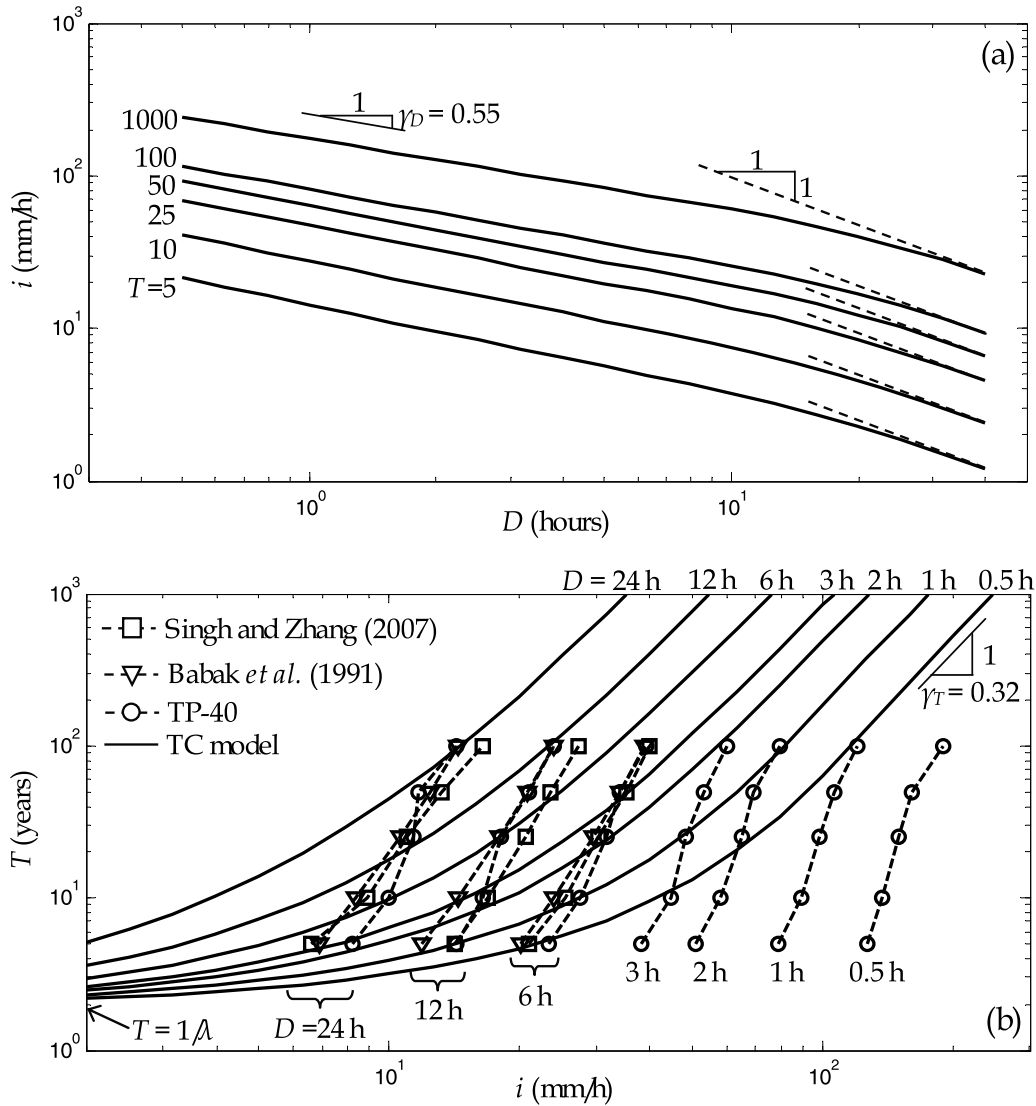


**Figure 9.** Theoretical IDF curves for New Orleans obtained from equation (11). (a) Maximum rainfall intensity  $i$  as a function of averaging duration  $D$  for different return periods  $T$ . (b) Comparison of the IDF values in Figure 9a for different averaging durations  $D$  (solid lines) with intensities obtained from continuous rainfall records.

[44] For short averaging durations (e.g.,  $D$  on the order of 1 h), the contribution of tropical cyclone rainfall to the risk is negligible, irrespective of the return period. A possible explanation is that (1) for short averaging durations  $D$ , extreme rainfalls are contributed by localized downpours caused by deep cumulus convection and (2) deep cumulus convection in TCs has many similarities with tropical cumulus clouds [see, e.g., Parrish *et al.*, 1984; Jorgensen *et al.*, 1985; Burpee, 1986; Powell, 1990] (among others). One concludes that for short  $D$  rainfall risk is dominated by storm types whose rate of occurrence is much higher than that of TCs.

[45] It is also of interest to determine which tropical cyclones contribute the most to the IDF values  $i(D, T)$ . Such TCs might for example be used as scenario events when designing for return period  $T$ . The main parameters to be considered are  $\theta = [V_{\max}, R_{\max}, V_i]$  and the distance  $y$  to the cyclone center. Their modal (most likely) values are obtained by maximizing the conditional probability density

of  $(y, \theta)$  given  $I_{D,\max} > i(D, T)$ . This conditional density is given by

$$f_{y,\theta|D,T}(y, \theta) \propto f_{y,\theta}(y, \theta) P[I_{D,\max}(y, \theta) > i(D, T)] \quad (15)$$

Figure 10 shows the modal values of  $V_{\max}$ ,  $R_{\max}$ , and  $V_i$  for different  $D$  and  $T$ . The most likely distance  $y$  always satisfies  $y \approx R_{\max}$ . This makes sense because  $R_{\max}$  is the distance at which the MSR model predicts maximum large-scale rainfall intensities.

[46] Figure 10a shows that the mode of  $V_{\max}$  increases when either  $D$  or  $T$  increase. This makes physical sense since for any given  $D$ , higher rainfall intensities require more intense storms, and for any given  $T$ , intense precipitation over longer averaging durations is associated with more intense systems. Figure 10b shows that the mode of  $V_i$  decreases as  $T$  increases, meaning that more intense rainfall is generally produced by slower-moving systems. For

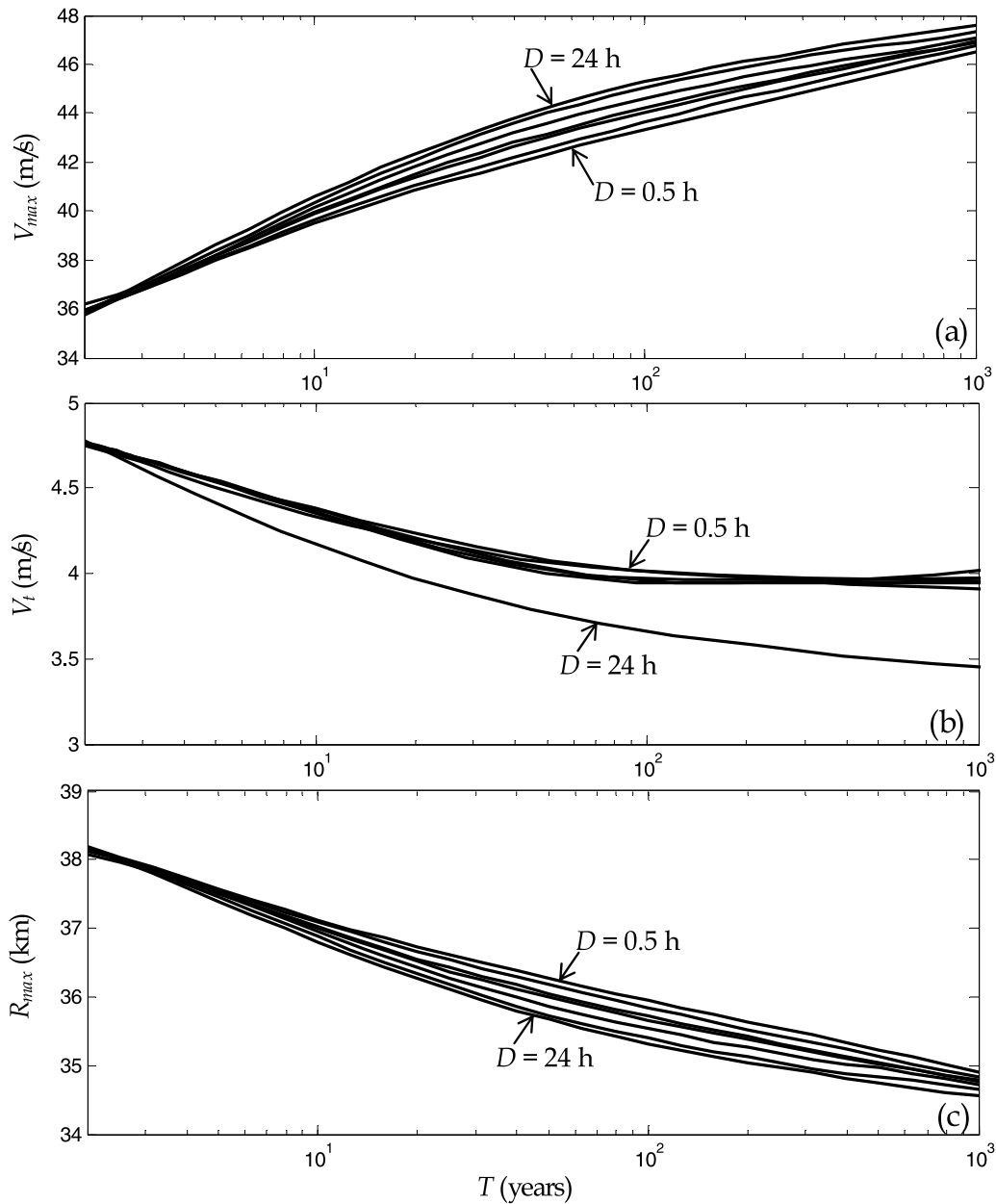


**Figure 10.** Modal values of (a)  $V_{max}$ , (b)  $V_t$ , and (c)  $R_{max}$  conditioned on exceeding the  $T$  year rainfall intensity for averaging duration  $D = 0.5, 1, 3, 6, 12,$  and  $24$  h.

averaging durations smaller than 12 h, the modal value of  $V_t$  is insensitive to  $D$ , whereas for longer averaging durations  $V_t$  decreases faster with  $T$ . This faster decay is related to the fact that, for averaging durations  $D$  on the order of 1 day or longer, extremely high rainfall intensities are produced by storms that take a time close to  $D$  to pass over the site. Therefore, for  $T$  large the translation speed  $V_t$  tends to be inversely proportional to  $D$ . Finally, Figure 10c shows that the mode of  $R_{max}$  decreases when either  $D$  or  $T$  increase. This makes sense, since more intense storms tend to have smaller values of  $R_{max}$ ; see section 5.1.

## 6. Conclusions

[47] We have developed a methodology to assess the frequency of extreme rainfall intensities from tropical cyclo-

nes (TCs) in coastal areas with flat topography. The mean rainfall field associated with a TC with maximum tangential wind speed  $V_{max}$ , radius of maximum winds  $R_{max}$ , and translation speed  $V_t$  is obtained using a physically based (“MSR”) model [Langousis and Veneziano, 2009], whereas rainfall variability at both large scales (from storm to storm) and small scales (due to rainbands and local convection within a single storm) is modeled statistically. The statistical component of the model is estimated using 38 precipitation radar (PR) frames from the TRMM mission; see Table 1. These frames cover a wide range of TC intensities  $V_{max}$  and vortex sizes  $R_{max}$ . To make the model easier to use in risk analysis, we developed approximate analytical expressions for the statistical parameters. We use Taylor’s hypothesis to convert spatial rainfall intensity fluctuations to temporal fluctuations as the storm passes over a given geographical

location A. The combined physical-statistical model predicts the maximum rainfall intensity at A during an averaging period  $D$  for a TC with characteristics  $(V_{\max}, R_{\max}, V_i)$  whose center passes at distance  $y$  from A. To illustrate the use of the model for long-term rainfall risk analysis, we formulated a recurrence model for tropical cyclones in the Gulf of Mexico that make landfall between longitudes  $85^\circ$  and  $95^\circ\text{W}$  and used the rainfall and recurrence models to assess the rainfall risk for New Orleans. Our main findings are as follows.

[48] The maximum rainfall  $I_{l,\max}$  in a spatial interval of length  $l$  depends on  $l$ , the distance  $y$  from the center of the TC, and the intensity  $V_{\max}$  and size  $R_{\max}$  of the vortex. We expressed  $I_{l,\max}$  as the product of the large-scale ( $L \approx 400$  km) average rainfall intensity produced by the MSR model,  $I_{L,MSR}$ , and an amplification factor  $\beta_{l,\max}$  that includes both storm-to-storm variability and spatial fluctuations of rainfall intensity within a storm. The distribution of  $\beta_{l,\max}$  depends of course on  $l$ , but in addition depends significantly on the large-scale intensity  $I_{L,MSR}$  and the standardized distance from the storm center,  $y' = |y/R_{\max}|$ . Specifically, the dispersion of  $\beta_{l,\max}$  increases as  $l$  and  $I_{L,MSR}$  decrease or  $y' = |y/R_{\max}|$  increases. These trends with  $I_{L,MSR}$  and  $y'$  are linked to the fact that lower-intensity storms and larger-distances  $y$  are associated with higher dry area fractions, more intermittent rainfall, and therefore an increased dispersion of the rainfall maxima.

[49] Application of the model to TC rainfall risk for New Orleans has produced interesting insight into the importance of tropical cyclones relative to other rainfall-producing events. For short return periods  $T$ , the TC intensities are significantly below those from other storms, which have a much higher rate of occurrence. However, as the return period  $T$  increases, the TC estimates for long averaging durations ( $D$  around 12–24 h) approach the values found from continuous rainfall records. This means that for long return periods, the long-duration TC rainfalls tend to dominate. In New Orleans, this happens for  $T$  around 100 years.

[50] To determine how the most likely TC scenario varies with the averaging duration  $D$  and the return period  $T$ , we calculated the joint distribution of  $\{V_{\max}, R_{\max}, V_i, y\}$  conditioned on exceeding the  $T$  year rainfall intensity for averaging duration  $D$ . Then we plotted the modal values of  $V_{\max}$ ,  $R_{\max}$ , and  $V_i$  against  $D$  and  $T$ ; see Figure 10 (for  $y$ , the modal value is always close to  $R_{\max}$ ). The modal value of  $V_{\max}$  increases when  $D$  or  $T$  increase, whereas the opposite is true for  $R_{\max}$ . The mode of the translation velocity  $V_i$  is insensitive to  $D$  for  $D < 24$  h, but decreases with increasing  $T$  and with increasing  $D$  for  $D > 24$  h.

[51] A rich parameterization and high computational efficiency make the proposed model attractive for rainfall risk applications in TC-prone areas. A limitation of the current model is that it does not account for landfall effects and therefore is applicable only to open water or coastal sites with flat topography. Future work should focus on extending the model to include inland conditions and extratropical conversion using coastal and over-land weather radar data.

[52] **Acknowledgments.** This work was supported by the Alexander S. Onassis Public Benefit Foundation under scholarship F-ZA 054/2005–2006. The authors are grateful to Shuyi Chen for the PR-TRMM rainfall products and Mark DeMaria for access to the extended best track record.

We also thank Demetris Koutsoyiannis and two anonymous reviewers for their useful comments and suggestions.

## References

- Atkinson, G. D., and C. R. Holiday (1977), Tropical cyclone minimum sea level pressure-maximum sustained wind relationship for western North Pacific, *Mon. Weather Rev.*, *105*, 421–427, doi:10.1175/1520-0493(1977)105<0421:TCMSLP>2.0.CO;2.
- Babak, N., V. P. Singh, and F. X. Yu (1991), LADOTD 24-hour rainfall frequency maps and IDF curves, La. Transp. Res. Cent., Baton Rouge.
- Bolen, S. M., and V. Chandrasekar (2000), Quantitative cross validation of space-based and ground-based radar observations, *J. Appl. Meteorol.*, *39*, 2071–2079, doi:10.1175/1520-0450(2001)040<2071:QCVOSB>2.0.CO;2.
- Burpee, R. W. (1986), Mesoscale structure of hurricanes, in *Mesoscale Meteorology and Forecasting*, edited by P. S. Ray, Am. Meteorol. Soc., Boston, Mass.
- Chen, S. S., M. Lonfat, J. A. Knaff, and F. D. Marks, Jr. (2006), Effects of vertical wind shear and storm motion on tropical cyclone rainfall asymmetries deduced from TRMM, *Mon. Weather Rev.*, *134*, 3190–3208, doi:10.1175/MWR3245.1.
- Chouinard, L. E., C. Liu, and C. K. Cooper (1997), Model for severity of hurricanes in Gulf of Mexico, *J. Waterw. Port Coastal Ocean Eng.*, *123*(3), 120–129, doi:10.1061/(ASCE)0733-950X(1997)123:3(120).
- Chow, V. T., D. R. Maidment, and L. W. Mays (1988), *Applied Hydrology*, McGraw-Hill, New York.
- Deidda, R., M. Grazia-Badas, and E. Piga (2006), Space–time multifractality of remotely sensed rainfall fields, *J. Hydrol. Amsterdam*, *322*, 2–13, doi:10.1016/j.jhydrol.2005.02.036.
- Demuth, J., M. DeMaria, and J. A. Knaff (2006), Improvement of Advanced Microwave Sounding Unit tropical cyclone intensity and size estimation algorithms, *J. Appl. Meteorol.*, *45*, 1573–1581, doi:10.1175/JAM2429.1.
- Ferraro, R., P. Pellegrino, M. Turk, W. Chen, S. Qiu, R. Kuligowski, S. Kusselson, A. Irving, S. Kidder, and J. Knaff (2005), The Tropical Rainfall Potential (TRaP) technique. Part II: Validation, *Weather Forecast.*, *20*, 465–475, doi:10.1175/WAF861.1.
- Gebremichael, M., T. M. Over, and W. F. Krajewski (2006), Comparison of the scaling properties of rainfall derived from space- and surface-based radars, *J. Hydrometeorol.*, *7*, 1277–1294, doi:10.1175/JHM549.1.
- Herbert, P. J., J. D. Jarrell, and M. Mayfield (1997), The deadliest, costliest, and most intense United States hurricanes of this century (and other frequently requested hurricane facts), *NOAA Tech. Memo. NWS-TPC-1*, Natl. Oceanic and Atmos. Admin., Miami, Fla.
- Hershfield, D. M. (1961), Rainfall frequency atlas for the United States for durations from 30 minutes to 24 hours and return periods from 1 to 100 years, *Tech. Pap. 40*, U.S. Weather Bur., Washington, D. C.
- Ho, F. P., and V. A. Myers (1975), Joint probability method of tide frequency analysis applied to Apalachicola Bay and St. George Sound, Florida, *NOAA Tech. Rep. NWS-18*, 43 pp., Natl. Oceanic and Atmos. Admin., Miami, Fla.
- Ho, F. P., J. C. Su, K. L. Hanevich, R. J. Smith, and F. P. Richards (1987), Hurricane climatology for the Atlantic and Gulf Coasts of the United States, *NOAA Tech. Rep. NWS-38*, 194 pp., Natl. Oceanic and Atmos. Admin., Miami, Fla.
- Holland, G. J. (1980), An analytic model of the wind and pressure profiles in hurricanes, *Mon. Weather Rev.*, *108*, 1212–1218, doi:10.1175/1520-0493(1980)108<1212:AAMOTW>2.0.CO;2.
- Interagency Performance Evaluation Taskforce (IPET) (2006), Engineering and operational risk and reliability analysis, vol. VIII, Technical appendix J, 60% progress report, U.S. Army Corps of Eng., Vicksburg, Miss.
- Interagency Performance Evaluation Taskforce (IPET) (2008), Engineering and Operational Risk and Reliability Analysis, vol. VIII, Technical appendix 8, hazard analysis, U.S. Army Corps of Eng., Vicksburg, Miss. (Available at <https://ipet.wes.army.mil/>)
- Jarvinen, B. R., C. J. Neumann, and M. A. S. Davis (1984), A tropical cyclone data tape for the North Atlantic Basin 1886–1993: Contents, limitations and uses, *NOAA Tech. Memo. NWS-NHC-22*, U.S. Dep. of Commer., Washington, D. C.
- Jorgensen, D. P., E. J. Zipser, and M. A. Lemone (1985), Vertical motions in intense hurricanes, *J. Atmos. Sci.*, *42*, 839–856, doi:10.1175/1520-0469(1985)042<0839:VMIIIH>2.0.CO;2.
- Kidder, S. Q., S. J. Kusselson, J. A. Knaff, R. R. Ferraro, R. J. Kuligowski, and M. Turk (2005), The Tropical Rainfall Potential (TRaP) technique, Part I, *Weather Forecast.*, *20*, 456–464, doi:10.1175/WAF860.1.
- Koutsoyiannis, D., D. Kozonis, and A. Manetas (1998), A mathematical framework for studying rainfall intensity-duration-frequency relation-

- ships, *J. Hydrol. Amsterdam*, 206, 118–135, doi:10.1016/S0022-1694(98)00097-3.
- Kummerow, C., W. Barnes, T. Kozu, J. Shiue, and J. Simpson (1998), The Tropical Rainfall Measuring Mission (TRMM) sensor package, *J. Atmos. Oceanic Technol.*, 15, 809–817, doi:10.1175/1520-0426(1998)015<0809:TTRMMT>2.0.CO;2.
- Langousis, A. (2008), Modeling long-term rainfall risk for tropical cyclones, Ph.D. thesis, Dep. of Civil and Environ. Eng., Mass. Inst. of Technol., Cambridge.
- Langousis, A., and D. Veneziano (2009), Theoretical model of rainfall in tropical cyclones for the assessment of long-term risk, *J. Geophys. Res.*, 114, D02106, doi:10.1029/2008JD010080.
- Langousis, A., D. Veneziano, P. Furcolo, and C. Lepore (2007), Multifractal rainfall extremes: Theoretical analysis and practical estimation, *Chaos Solitons Fractals*, doi:10.1016/j.chaos.2007.06.004.
- Langousis, A., D. Veneziano, and S. Chen (2008), Boundary layer model for moving tropical cyclones, in *Hurricanes and Climate Change*, edited by J. Elsner and T. H. Jagger, Springer, New York.
- Lee, T. F., F. J. Turk, J. Hawkins, and K. Richardson (2002), Interpretation of TRMM TMI images of tropical cyclones, *Earth Interact.*, 6, 1–17, doi:10.1175/1087-3562(2002)006<0001:IOTTIO>2.0.CO;2.
- Liao, L., R. Meneghini, and T. Iguchi (2001), Comparisons of rain rate and reflectivity factor derived from the TRMM precipitation radar and the WSR-88D over the Melbourne, Florida, site, *J. Atmos. Oceanic Technol.*, 18, 1959–1974, doi:10.1175/1520-0426(2001)018<1959:CORRAR>2.0.CO;2.
- Lonfat, M., F. D. Marks, Jr., and S. S. Chen (2004), Precipitation distribution in tropical cyclones using the Tropical Rainfall Measuring Mission (TRMM) microwave imager: A global perspective, *Mon. Weather Rev.*, 132, 1645–1660, doi:10.1175/1520-0493(2004)132<1645:PDITCU>2.0.CO;2.
- Lonfat, M., R. Rogers, T. Marchok, and F. D. Marks, Jr. (2007), A parametric model for predicting hurricane rainfall, *Mon. Weather Rev.*, 135, 3086–3097, doi:10.1175/MWR3433.1.
- Madsen, H., P. F. Rasmussen, and D. Rosbjerg (1997), Comparison of annual maximum series and partial duration series methods for modeling extreme hydrologic events: 1. At-site modeling, *Water Resour. Res.*, 33(4), 747–757, doi:10.1029/96WR03848.
- Marks, F. D., G. Kappler, and M. DeMaria (2002), Development of a tropical cyclone Rainfall Climatology and Persistence (RCLIPER) model, paper presented at 25th Conference on Hurricanes and Tropical Meteorology, Am. Meteor. Soc., San Diego, Calif.
- Molinari, J., P. K. Moore, V. P. Idone, R. W. Henderson, and A. B. Saljoughy (1994), Cloud-to-ground lightning in Hurricane Andrew, *J. Geophys. Res.*, 99, 16,665–16,676, doi:10.1029/94JD00722.
- Myers, V. A. (1975), Storm tide frequencies on the South Carolina coast, *NOAA Tech. Rep. NWS-16*, 79 pp., Natl. Oceanic and Atmos. Admin., Miami, Fla.
- Over, T. M., and V. K. Gupta (1996), A space-time theory of mesoscale rainfall using random cascades, *J. Geophys. Res.*, 101(D21), 26,319–26,331, doi:10.1029/96JD02033.
- Parrish, J. R., R. W. Burpee, F. D. Marks, Jr., and C. W. Landsea (1984), Mesoscale and convective-scale characteristics of Hurricane Frederic during landfall, paper presented at 15th Conference of Hurricanes and Tropical Meteorology, Am. Meteor. Soc., Miami, Fla.
- Powell, M. (1990), Boundary layer structure and dynamics in outer hurricane rainbands. Part I: Mesoscale rainfall and kinematic structure, *Mon. Weather Rev.*, 118, 891–917, doi:10.1175/1520-0493(1990)118<0891:BLSADI>2.0.CO;2.
- Powell, M., G. Soukup, S. Cocks, S. Gulati, N. Morisseau-Leroy, S. Hamid, N. Dorst, and L. Axe (2005), State of Florida hurricane loss projection model: Atmospheric science component, *J. Wind Eng. Ind. Aerodyn.*, 93, 651–674, doi:10.1016/j.jweia.2005.05.008.
- Rappaport, E. N. (2000), Loss of life in the United States associated with recent Atlantic tropical cyclones, *Bull. Am. Meteorol. Soc.*, 81, 2065–2074, doi:10.1175/1520-0477(2000)081<2065:LOLITU>2.3.CO;2.
- Scofield, R. A., and R. J. Kuligowski (2003), Status and outlook of operational satellite precipitation algorithms for extreme precipitation events, *Weather Forecast.*, 18, 1037–1051, doi:10.1175/1520-0434(2003)018<1037:SAOOOS>2.0.CO;2.
- Shen, W. (2006), Does the size of hurricane eye matter with its intensity?, *Geophys. Res. Lett.*, 33, L18813, doi:10.1029/2006GL027313.
- Simpson, J., R. F. Adler, and G. R. North (1988), Proposed Tropical Rainfall Measuring Mission (TRMM) satellite, *Bull. Am. Meteorol. Soc.*, 69, 278–295, doi:10.1175/1520-0477(1988)069<0278:APTRMM>2.0.CO;2.
- Singh, V. P. (1992), *Elementary Hydrology*, Prentice-Hall, Upper Saddle River, N. J.
- Singh, V. P., and L. Zhang (2007), IDF curves using the Frank Archimedean copula, *J. Hydrol. Eng.*, doi:10.1061/(ASCE)1084-0699(2007)12:6(651).
- Smith, R. K. (1968), The surface boundary layer of a hurricane, *Tellus*, 20, 473–484.
- Taylor, G. I. (1921), Diffusion processes by continuous movements, *Proc. London Math. Soc.*, 20(2), 196–211.
- Taylor, G. I. (1938), The spectrum of turbulence, *Proc. R. Soc. London, Ser. A*, 164, 476–490.
- Tuleya, R. E., M. DeMaria, and J. R. Kuligowski (2007), Evaluation of GFDL and simple statistical model rainfall forecasts for U.S. landfalling tropical storms, *Weather Forecast.*, 22, 56–70, doi:10.1175/WAF972.1.
- Veneziano, D., P. Furcolo, and V. Iacobellis (2006a), Imperfect scaling of time and space-time rainfall, *J. Hydrol. Amsterdam*, 322(1–4), 105–119, doi:10.1016/j.jhydrol.2005.02.044.
- Veneziano, D., A. Langousis, and P. Furcolo (2006b), Multifractality and rainfall extremes: A review, *Water Resour. Res.*, 42, W06D15, doi:10.1029/2005WR004716.
- Vicente, G. A., R. A. Scofield, and W. P. Menzel (1998), The operational GOES infrared rainfall estimation technique, *Bull. Am. Meteorol. Soc.*, 79, 1883–1898, doi:10.1175/1520-0477(1998)079<1883:TOGIRE>2.0.CO;2.
- Vickery, P. J., and L. A. Twisdale (1995), Prediction of hurricane wind speeds in the United States, *J. Struct. Eng.*, 121(11), 1691–1699, doi:10.1061/(ASCE)0733-9445(1995)121:11(1691).
- Vickery, P. J., P. F. Skerlj, and L. A. Twisdale (2000), Simulation of hurricane risk in the U.S. using empirical track model, *J. Struct. Eng.*, 126(10), 1222–1237, doi:10.1061/(ASCE)0733-9445(2000)126:10(1222).
- Willoughby, H. E., and M. E. Rahn (2004), Parametric representation of the primary hurricane vortex. Part I: Observations and evaluation of the Holland (1980) model, *Mon. Weather Rev.*, 132, 3033–3048, doi:10.1175/MWR2831.1.
- Wolff, D. B., D. A. Marks, E. Amitai, D. S. Silberstein, B. L. Fisher, A. Tokay, J. Wang, and J. L. Pippitt (2005), Ground validation for the Tropical Rainfall Measuring Mission (TRMM), *J. Atmos. Oceanic Technol.*, 22, 365–380, doi:10.1175/JTECH1700.1.

---

A. Langousis and D. Veneziano, Department of Civil and Environmental Engineering, Massachusetts Institute of Technology, Room 1-245, Cambridge, MA 02139, USA. (andlag@mit.edu)